RSC Advances

ROYAL SOCIETY OF CHEMISTRY

www.rsc.org/advances

Revised manuscript submitted to RSC Advances

Date: February 21, 2015

Role of Acid Sites and Surface Hydroxyl Groups in Isophthalonitrile Hydrogenation Catalyzed by Supported Ni-Co Catalysts

Chang Liu, Ruijun Hou, Tiefeng Wang*

Beijing Key Laboratory of Green Reaction Engineering and Technology

Department of Chemical Engineering, Tsinghua University, Beijing 100084, China

**Corresponding author: 86-10-62794132, wangtf@tsinghua.edu.cn*

Abstract

Meta-xylylenediamine (*m*-XDA) is industrially produced by the hydrogenation of isophthalonitrile (IPN) using Raney Ni/Co and basic additives. Compared with Raney Ni/Co, the supported Ni/Co catalysts are safer and have better mechanical strength. This work aimed to study the catalytic performance of the supported Ni-Co catalysts in hydrogenation of IPN to *m*-XDA. The active sites for the condensation side reactions were studied using Ni-Co catalysts supported on different oxides and with different loadings. It was found that the acid sites catalyzed the condensation reactions between intermediate imines and amines. Two types of acid sites existed on the supported Ni-Co catalysts, namely, the original acid sites of the support and new acid sites formed by Ni/Co aluminates. In addition to acid sites, the surface hydroxyl groups on the oxide supports also catalyzed the condensation reactions, but which were not active for the hydrogenation reaction. By increasing the Ni-Co loading, the selectivity to *m*-XDA was significantly enhanced, which was attributed to the suppression of both acid sites and hydroxyl groups. Compared to the low-loading catalysts (5Ni-1.25Co/Al_2O_3 and 5Ni-1.25Co/SiO_2), the high-loading catalysts (20Ni-5Co/Al_2O_3 and 20Ni-5Co/SiO_2) increased the *m*-XDA selectivity from ~45.5% to 99.9%.

Keywords: IPN hydrogenation, Ni-Co supported catalyst, metal loading, catalyst acidity, surface hydroxyl groups

Introduction

Meta-xylylenediamine (*m*-XDA) is an important fine chemical intermediate that is widely used in the production of pharmaceuticals, disinfectants, rubber stabilizers, textile additives and curing agents of epoxy [1, 2]. The industrial production of *m*-XDA uses the hydrogenation of isophthalonitrile (IPN) catalyzed by Raney Ni/Co catalysts with basic additives [1-3]. Raney Ni/Co catalysts have a high selectivity to *m*-XDA [4-7], which can be further enhanced by adding other metal components [1]. Although the skeleton structure of Raney catalysts favors a high catalytic activity, it causes low mechanical strength and bad regeneration capability, leading to a very high catalyst consumption [8]. In addition, a safety hazard also exists as the Raney catalysts are flammable when exposed to air. Recently, the supported metal catalysts with metals from Group VIII such as Pd, Pt, Ru, Ni and Co as the active component have attracted more attentions [2, 9-15]. The supported catalysts have good mechanical strength provided by the support, and the *m*-XDA selectivity can be enhanced by optimizing both the metal composition and the support [14, 16-19]. Among Group VIII metals, Ni and Co give high selectivity to *m*-XDA and a synergy effect of the Ni-Co bimetal can further enhance the catalytic performance. A variety of oxides can be used as the support, among which γ-Al_2O_3, SiO_2 and MgO are the most widely used [2, 15, 20, 21]. The product selectivity is also affected by the metal loading. A high metal loading (> 10 wt%) of the Ni-based supported catalyst is usually used to give a high selectivity (> 90%) to primary amines [2, 9, 13-15]. However, the underlying mechanism has not been studied.

According to the reaction routes shown in Scheme 1 [6, 9, 22, 23], in addition to the hydrogenation reactions, condensation reactions between the highly reactive intermediate imines and amines are the main side reactions in IPN hydrogenation. The condensation reactions decrease the selectivity

to *m*-XDA and cause catalyst deactivation by forming higher amines and blocking the catalytic sites. The bifunctional mechanism [17] reveals that in a nitrile hydrogenation system, the hydrogenation reactions are catalyzed by metal sites while condensation reactions are catalyzed by acid sites. It was confirmed by the studies of Verhaak et al. [17], Infantes-Molina et al. [19], Cabello et al. [24] and Chen et al. [20] that the acid-base properties of the support are crucial to the catalytic performance. The surface acidity favors the conversion of nitrile but decreases the selectivity to primary amines, and the surface basicity shows the opposite effects. Actually, oxide surfaces are usually covered by hydroxyl groups, which are potential proton donors or acceptors [25-27], and play an important role in the adsorption property and catalytic performance [28, 29]. However, the acid-basic property of the surface hydroxyl groups highly depends on the environment [30]. Unless activated by agents [31], the surface hydroxyl groups on SiO_2 and γ-Al_2O_3 are very stable and do not show Brønsted acidity and basicity by providing H^+ or OH^-. In addition to the acid-basic property of the support, a metal-support interaction also affects the catalytic performance. Rode et al. [18] studied a series of supported Ni catalysts and reported that the Ni dispersion depends on the support. For the gas-phase hydrogenation of benzonitrile and acetonitrile, the total catalytic activity increases with decreasing Ni dispersion. Gluhoi et al. [32] revealed that new active sites formed at the metal-support interface enhanced the activity of supported Ni catalysts in acetonitrile hydrogenation. The results in the literatures suggest that the support affects the catalytic performance by providing original acid sites, modulating the dispersion of active metal and forming new active sites. However, the mechanism of the formation of new acid sites and their effects are still unclear. The effect of the nature of support on the catalyst composition and catalytic performance is also not well known.

In this work, a series of γ-Al_2O_3 and SiO_2 supported Ni-Co catalysts with different metal loading were synthesized and evaluated for IPN hydrogenation. MgO supported catalysts were also tested for comparison. The preparation method was optimized to enhance the metal dispersion and catalytic performance. The effects of preparation method, Ni-Co loading and nature of support on the catalyst acidity and catalytic performance, and the effect of acid sites and surface hydroxyls groups on the side reactions were systematically studied.

2. Experimental

2.1 Catalyst preparation

A series of Ni-Co supported catalysts, *x*Ni-*y*Co/Al_2O_3 and *x*Ni-*y*Co/SiO_2 (*x, y* are the Ni and Co loading in wt%), were prepared by incipient wetness impregnation using nitrates ($Ni(NO_3)_2{\cdot}6H_2O$, 98%, Alfa Aesar, $Co(NO_3)_2{\cdot}6H_2O$, 98.0%, Alfa Aesar) as the metallic precursors and γ-Al_2O_3 or SiO_2 (Alfa Aesar, both ground to 40–80 mesh) as the support. The mass ratio of Ni to Co was kept at 4:1, and the Ni loading was varied from 2.5 to 20 wt% (x = 2.5–20, y = 0.625–5). Ni and Co were impregnated onto the support simultaneously. The impregnated samples were treated with an ultrasonic treatment for 1 h to facilitate metal dispersion, and were aged overnight at room temperature. Then the catalyst samples were dried in air at 80 ^{o}C for 6 h and calcined at 400 ^{o}C for 4 h.

Because the solubility of the nitrates and the water absorption capacity of the supports were low, the catalysts with high Ni-Co loadings, 10Ni-2.5Co/Al_2O_3, 20Ni-5Co/Al_2O_3, 10Ni-2.5Co/SiO_2 and 20Ni-5Co/SiO_2, could not be prepared in one impregnation. In this work, repeated impregnation (RI method) of a calcined catalyst with a lower Ni-Co loading was used to prepare the catalysts with loading of x = 10 and 20. For x = 10, the required amount of Ni and Co

nitrate solution was divided into two portions, and used to impregnate the support two times. For *x* = 20, the catalyst preparation used four impregnations. For comparison, a single step impregnation (SI method) was also used to prepare 20Ni-5Co/Al_2O_3 and 20Ni-5Co/SiO_2. In the SI method, the nitrate solution was added to the support four times with drying at 80 ^oC in air after each impregnation, and then the sample was calcined. These were denoted as 20Ni-5Co/Al_2O_3(SI) and 20Ni-5Co/SiO_2(SI). The MgO supported catalysts were prepared similarly. The catalysts obtained were stored in vials and pre-reduced in H_2 flow (70 ml min^{-1}) at 450 ^oC for 5 h and passivated in N_2 flow before being used in the hydrogenation reactions.

2.2 Catalyst characterization

The BET surface area, pore volume and pore size distribution of the unreduced catalysts and the supports were measured by N_2 adsorption with a Quantachrome Autosorb iQ and AsiQwin instrument. The X-ray diffraction (XRD) patterns of the unreduced and reduced catalysts and supports were recorded on a Bruker D8 Advance powder X-ray diffratomer (40 kV, 40 mA) with a Cu K_α radiation source and a Ni filter in the 2θ range of 5–90 ^{o}. Scanning electron microscopy (SEM, JEOL JEM-7401F) was used to observe the morphology of the unreduced catalysts and supports.

The reducibility of the catalysts was tested by temperature programmed reduction (H_2-TPR) performed on a Quantachrome ChemBET Pulsar TPR/TPD instrument. A 5% H_2/Ar mixture was used as the reducing gas. The consumption of H_2 was measured by a TCD. Ammonia temperature programmed desorption (NH_3-TPD) was also conducted on the Quantachrome ChemBET Pulsar TPR/TPD instrument. The catalysts were reduced at 450 ^oC online before the measurement. A mixture of 5% NH_3/He was used for the adsorption, and the signal of ammonia desorption was

recorded by a TCD. The acidic properties of some selected catalysts were also characterized by FT-IR spectroscopic analysis. The spectra were recorded with a NICOLET 6700 spectrometer equipped with a heatable IR cell with KBr windows, connected to a gas dosing-evacuating system. The surface hydroxyl content of the support was determined by thermogravimetric analysis (TG-DTA) on a NETZSCH STA 409PC in N_2. The support powders were heated from 30 ^oC to 120 ^oC at 10 °C min^{-1} and held at 120 ^oC for 10 min to remove the physically adsorbed water, and then the sample was heated to 800 °C min^{-1} at 20 °C min^{-1} and held for 10 min. The surface hydroxyl content of the supports was calculated according to weight loss in the second heating step [33]. The coke properties of the spent catalysts were also determined by TG-DTA with an O_2 flow of 50 mL min^{-1}.

2.3 Catalytic reaction

The catalysts were evaluated for the hydrogenation of IPN in a stainless steel autoclave (Weihai Chemical Machinery Co., Ltd., 250 mL). To eliminate the influence of external and internal diffusion, the stirring speed of the magnetically driven impeller was set at 800 rpm, and the H_2 flow rate was set at 190 mL min^{-1} by a mass flow meter. The reaction temperature was 80 ^oC and the pressure was 6.0 MPa. A mixture of 20 mL methanol (> 99.5%, Beijing Chemical Works) and 80 mL toluene (> 99.5%, Beijing Modern Oriental Fine Chemistry Co., Ltd.) was used as the solvent, and 0.086 g NaOH (> 96.0%, Beijing Chemical Works) was used as a basic additive. For each experiment, the amount of IPN (98%, J&K Chemical) was 2.9 g. The amount of catalyst was adjusted to give 0.25 g Ni and 0.0625 g Co on the catalyst:

$$\text{Catalyst mass} = \frac{25}{x} \text{ or } \frac{6.25}{y} \quad (x, y \text{ in wt\%}) \tag{1}$$

Before each experiment, the catalyst was pre-reduced in H_2 flow of 70 ml min^{-1} at 450 ^oC for

5 h. After passivation in N_2 flow, the reduced catalyst was transferred to the reactant solution in the autoclave. The system was purged with H_2 flow for 30 min under 300 rpm stirring to displace trapped air. Then the reactor system was heated to 80 ^oC under 0.3 MPa and pressurized to 6.0 MPa within 5 min while the H_2 flow rate and stirring speed were set to the specified values. The time when the pressure reached 6.0 MPa was considered as the zero time of the reaction.

The products were sampled online at time intervals of 10 min and were analyzed by a gas chromatograph (GC 7900II, Techcomp Instrument Company) equipped with a DB-1MS UI capillary column (30 m × 0.25 mm × 0.25 μm, Agilent) and an FID detector. The conversion of IPN and the selectivity to *m*-XDA were calculated as:

$$\text{IPN conversion}=\frac{\text{moles of converted IPN}}{\text{moles of IPN feedstock}}\times 100\% \quad (2)$$

$$\text{Product selectivity}=\frac{\text{moles of carbon in a defined product}}{\text{moles of carbon in converted IPN}}\times 100\% \quad (3)$$

The higher amines and other oligomers in the liquid samples could not be detected by GC. To identify the heavier species, some liquid samples were analyzed by mass spectrometry (MS, instrument model: Q Exactive).

3. Results and discussion

3.1. Catalyst characterization

3.1.1. BET surface area

The physical properties of *x*Ni-*y*Co/Al_2O_3 and γ-Al_2O_3 (calcined before analysis) are listed in Table 1. The support γ-Al_2O_3 had a surface area of 221 $m^2 g^{-1}$ and a pore volume of 0.63 $cm^3 g^{-1}$, which decreased after the introduction of Ni-Co. As the Ni-Co loading increased from x = 0 to x = 20, the surface area decreased from 221 to 153 $m^2 g^{-1}$, and the pore volume decreased from 0.63 to

0.41 cm^3 g^{-1}, while the average pore diameter remained almost unchanged in the range of 7.88−7.92 nm. The BET results of *x*Ni-*y*Co/SiO_2 and SiO_2 are also included in Table 1. Overall, the SiO_2 supported catalysts had smaller specific surface areas, similar pore volumes and larger pore sizes compared to their counterparts on γ-Al_2O_3. The loading of Ni and Co decreased the surface area and pore volume. The surface area and pore volume of SiO_2 were 152 m^2 g^{-1} and 0.62 cm^3 g^{-1}, respectively, and the values for 20Ni-5Co/SiO_2 were 100 m^2 g^{-1} and 0.38 cm^3 g^{-1}, respectively. The pore size distribution was little changed with the loading of Ni and Co. In agreement with the results in the literature [15, 34], the BET results suggested the uniform dispersion of Ni-Co on the support, with part of the pore structure blocked by Ni-Co particles at high metal loadings.

3.1.2. XRD

The XRD patterns of γ-Al_2O_3 and the unreduced *x*Ni-*y*Co/Al_2O_3 catalysts are shown in Fig. 1(a). It was confirmed by the XRD and H_2-TPR (discussed below in 3.1.4) analysis that NiO, Co_3O_4, $NiCo_2O_4$ and Ni/Co aluminates were the main phases [35, 36]. The XRD patterns of γ-Al_2O_3 showed little change after the introduction of Ni-Co at loadings of $x \leq 5$. The results were attributed to the low Ni-Co loading and the overlapped peaks of Ni/Co oxides and γ-Al_2O_3. At the Ni-Co loading of $x > 5$, the characteristic peaks of NiO, Co_3O_4 and $NiCo_2O_4$ were detected. It should be pointed out that some characteristic peaks of Co_3O_4 and $NiCo_2O_4$ overlap each other, which made the two species hard to distinguish. However, the two species had some particular characteristic peaks besides the common peaks. In this study, the peak at 31° was used to analyze Co_3O_4 and the peak at 36° was used to analyze $NiCo_2O_4$. In addition, the two species were further confirmed by the different reducibility measured by H_2-TPR as discussed in 3.1.4. The crystal

sizes were estimated by the Scherrer equation and listed in Table 1. The crystal sizes of NiO, Co_3O_4 and $NiCo_2O_4$ were, respectively, 10.8, 20.9 and 17.4 nm on 10Ni-2.5Co/Al_2O_3, and were, respectively, 11.4, 21.0 and 16.9 nm on 20Ni-5Co/Al_2O_3. Compared with 20Ni-5Co/Al_2O_3, more NiO and Co_3O_4 and less $NiCo_2O_4$ were formed on 20Ni-5Co/Al_2O_3(SI), with much larger crystal sizes, which were 20.2, 32.2 and 29.6 nm for NiO, Co_3O_4 and $NiCo_2O_4$, respectively. For further comparison, the 20Ni-5Co/Al_2O_3 and 20Ni-5Co/Al_2O_3(SI) catalysts were analyzed after reduction. The Ni crystal particle size was 8.6 nm on reduced 20Ni-5Co/Al_2O_3, and it was 13.7 nm on 20Ni-5Co/Al_2O_3(SI). This trend was consistent with the results of the unreduced catalysts.

The XRD patterns of SiO_2 and *x*Ni-*y*Co/SiO_2 further confirmed the effects of Ni-Co loading and the preparation method on metal dispersion and formation of bimetallic oxides. These are shown in Table 1 and Fig. 1(b). Similar to the γ-Al_2O_3 supported catalysts, NiO, Co_3O_4, $NiCo_2O_4$ and the Ni/Co silicates were the main phases of Ni and Co on *x*Ni-*y*Co/SiO_2. The *x*Ni-*y*Co/SiO_2 catalysts at the loading of x = 2.5–20 had similar average crystal sizes of Ni-Co oxides, while 20Ni-5Co/SiO_2(SI) had more NiO and Co_3O_4, less $NiCo_2O_4$, and lower metal dispersion.

The crystal sizes of the *x*Ni-*y*Co/SiO_2 catalysts were considerably larger than those of the *x*Ni-*y*Co/Al_2O_3 catalysts. On average, for the Ni-Co/Al_2O_3 catalysts prepared by the RI method, the crystal sizes of NiO, Co_3O_4 and $NiCo_2O_4$ were 11.1, 21.0 and 17.2 nm, respectively. For the SiO_2 supported catalysts, the corresponding average crystal sizes were 21.1, 20.1 and 21.4 nm. In addition, more NiO and Co_3O_4 and less $NiCo_2O_4$ were formed on SiO_2 than on γ-Al_2O_3. These results indicated that the RI method using γ-Al_2O_3 as support facilitated the metal dispersion and formation of Ni-Co bimetallic oxides.

3.1.3. SEM results

Figure 2 shows the SEM images of γ-Al_2O_3 and the unreduced xNi-yCo/Al_2O_3 catalysts. The floccules in the image of γ-Al_2O_3 were due to the partially amorphous morphology of the support. After the loading of Ni-Co, no significant change in morphology was detected in the SEM images, except for 20Ni-5Co/Al_2O_3(SI), on which large octahedral crystal particles were observed. Consistent with the BET and XRD results, the SEM images show that Ni and Co were uniformly dispersed on the γ-Al_2O_3 support when the RI method was used. In contrast, aggregation of Ni/Co oxides was much more serious on 20Ni-5Co/Al_2O_3(SI) and this led to larger crystal particles.

The SEM results of the xNi-yCo/SiO_2 catalysts were similar to that of xNi-yCo/Al_2O_3 (Fig. S1). It was confirmed by the SEM images that the Ni-Co dispersion was uniform on the SiO_2 support for the catalysts prepared by the RI method, while for 20Ni-5Co/SiO_2(SI), large crystal particles were observed.

3.1.4. H_2-TPR results

The H_2-TPR profiles of the xNi-yCo/Al_2O_3 catalysts are shown in Fig. 3. The results of Ni/Al_2O_3 and Co/Al_2O_3 (both at the loading of 5.0 wt%) are also included for comparison. As shown in the H_2-TPR profiles of Ni/Al_2O_3 and Co/Al_2O_3, the reduction peaks of Ni oxide were at 450 and 700 ^oC, and that of Co oxide was at 475 ^oC. For all the xNi-yCo/Al_2O_3 catalysts, the reduction of Ni/Co oxides had two peaks at 370 and 650 ^oC, which were lower than the characteristic peaks of the monometallic Ni and Co catalysts. The H_2-TPR results indicated the formation of Ni-Co bimetallic oxides, which had a higher reducibility than the Ni and Co monometallic oxides.

The reduction peaks at 370 ^oC was attributed to the reduction of NiO, Co_3O_4 and $NiCo_2O_4$, and that at 650 ^oC was due to $NiAl_2O_4$ and $CoAl_2O_4$, which were less reducible [2]. With the

increase of Ni-Co loading, the single reduction peak at 370 °C splitted into two peaks and shifted slightly to higher temperature. The splitted peaks were due to the different compounds of Ni and Co, namely the monometallic oxides (NiO and Co_3O_4) and the bimetallic oxide ($NiCo_2O_4$), with the latter being more reducible. With the increase of Ni-Co loading, the ratio of NiO and Co_3O_4 to $NiCo_2O_4$ increased and the reducibility decreased. In addition, the reduction peak area increased with an increase in the Ni-Co loading due to the increased amount of the Ni and Co oxides. In the case of 20Ni-5Co/Al_2O_3(SI), the characteristic peaks of NiO, Co_3O_4 and Ni/Co aluminates were enhanced while that of $NiCo_2O_4$ was weakened. This further confirmed the formation of less $NiCo_2O_4$ and the lower metal dispersion on 20Ni-5Co/Al_2O_3(SI).

The dominant reduction peaks of *x*Ni-*y*Co/SiO_2 were below 600 °C, indicating the formation of less Ni and Co silicates on SiO_2. The peak at 300 °C was attributed to the reduction of $NiCo_2O_4$ and that at 400 °C was attributed to NiO and Co_3O_4. For the *x*Ni-*y*Co/SiO_2 catalysts prepared by the RI method, the peak locations and the relative peak areas were unchanged with the Ni-Co loading. In accordance with the XRD results, the H_2-TPR results demonstrated that there were less $NiCo_2O_4$ but more NiO and Co_3O_4 on SiO_2 than on γ-Al_2O_3. Overall, the surface composition of *x*Ni-*y*Co/SiO_2 was less dependent on the Ni-Co loading than that of *x*Ni-*y*Co/Al_2O_3.

3.1.5. Catalyst acidity

The reduced *x*Ni-*y*Co/Al_2O_3 catalysts and γ-Al_2O_3 were tested by NH_3-TPD. The total acidity of each catalyst and γ-Al_2O_3 was calculated from the desorbed amount of NH_3 corresponding to the desorption peak in the range of 100–500 °C (Fig. S2). The results are summarized in Table 2. The support γ-Al_2O_3 has some acidity generated from dehydration [37, 38]. The loading of Ni-Co significantly affected the acidity. With an increase in the Ni-Co loading, the total acidity increased

from 0.180 mmol NH_3 g^{-1} for γ-Al_2O_3 to 0.224 mmol NH_3 g^{-1} for 2.5Ni-0.625Co/Al_2O_3, and reached its maximum of 0.474 mmol NH_3 g^{-1} for 5Ni-1.25Co/Al_2O_3. With a further increase of the Ni-Co loading, the acidity decreased from 0.474 mmol NH_3 g^{-1} for 5Ni-1.25Co/Al_2O_3 to 0.160 mmol NH_3 g^{-1} for 20Ni-5Co/Al_2O_3. The poorly dispersed 20Ni-5Co/Al_2O_3(SI) had an acidity of 0.264 mmol NH_3 g^{-1}, which was larger than that of 20Ni-5Co/Al_2O_3. It was reported that the aluminates, $NiAl_2O_4$ and $CoAl_2O_4$, which were confirmed by XRD and H_2-TPR analysis in this work, were mainly responsible for the enhanced acidity [37, 39, 40]. In $NiAl_2O_4$ and $CoAl_2O_4$ spinel, the positive charge of the surface is higher than on γ-Al_2O_3, and is present in the form of Al^{3+} surface cations, which act as Lewis acid sites. Confirmed by the results of FT-IR (Fig. S3), all the acid sites on the reduced *x*Ni-*y*Co/Al_2O_3 catalysts and γ-Al_2O_3 were Lewis acid sites, consistent with the literature. However, the literatures [38, 40-42] had no consensus about the effects of the metal on the acidity. Some researchers reported that the introduction of Ni enhanced the acidity of alumina and silica-alumina support [40], while others reported the opposite effects [38, 41]. In other studies, more complicated effects were reported [42]. In this work, the enhanced acidity was attributed to the exposed Ni/Co aluminates. The newly formed acid sites only showed acidity when they were exposed without being covered by the loaded metals. Therefore, the Ni-Co loading had two effects on the catalyst acidity, namely, the formation and exposure of the Ni/Co aluminates. At the Ni-Co loadings of $x \leq 5$, the effect of aluminates formation was dominant, therefore the acidity increased with Ni-Co loading. As the Ni-Co loading further increased to $x > 5$, the decrease in exposure of the aluminates became dominant because some acid sites on the Ni/Co aluminates were covered by Ni-Co, therefore the acidity decreased with increasing Ni-Co loading.

The Ni-Co catalysts supported on SiO_2, a much less acidic support, were also analyzed by

NH_3-TPD, as shown in Table 2. The support SiO_2 had very low acidity of 0.014 mmol NH_3 g^{-1}, which was less than 10% of that of γ-Al_2O_3. At the Ni-Co loading of x = 2.5, the catalyst acidity increased to 0.087 mmol NH_3 g^{-1}. Further increase of the Ni-Co loading reduced the catalyst acidity to 0.023 mmol NH_3 g^{-1} at the Ni-Co loading of x = 20. Similar to the γ-Al_2O_3 supported catalysts, the preparation method also had effects on the catalyst acidity. The 20Ni-5Co/SiO_2(SI) catalyst had a stronger acidity than 20Ni-5Co/SiO_2. Nevertheless, all the Ni-Co/SiO_2 catalysts had much lower acidity than their counterparts on γ-Al_2O_3, due to the much less formation of Ni/Co silicates, which were the source of the new acid sites.

3.2. Catalytic performance

3.2.1. Effect of preparation method and Ni-Co loading

The γ-Al_2O_3 supported catalysts were evaluated for IPN hydrogenation under the same conditions to study the role of acid sites by using catalyst with different preparation methods and Ni-Co loadings. For each experiment, the catalyst amount used was adjusted to give the amounts of Ni and Co of 0.25 g and 0.0625 g, respectively. The conversion of IPN and selectivity to *m*-XDA are plotted as a function of reaction time in Fig. 4. The rate constant (k_r) for IPN hydrogenation and selectivity to *m*-XDA over xNi-yCo/Al_2O_3 based on the same metal amount are listed in Table 2. The reaction order (p) and rate constant (k_r) were determined by fitting the IPN concentration data in the first 100 min as a function of the reaction time using Eq. (4).

$$\frac{\mathrm{d}C_{IPN}}{\mathrm{d}t} = -k_r C_{IPN}^{p} \quad (4)$$

The reaction order of IPN was found to be in the range 0.75~0.85. To further quantitatively compare the activity of different catalysts, the reaction order was fixed at 0.8. With p = 0.8, Eq. (4)

has a good agreement with the experimental data of all the catalyst, with $R^2 \geq 0.99$. For comparison, the calculations with $p = 1.0$ were also included in Table S1. When the 1st order was used, there was a large deviation between the calculated and measured IPN concentrations for 5Ni-1.25Co/Al_2O_3 and 20Ni-5Co/Al_2O_3, with R^2 less than 0.95. The fitting results with $p = 0.8$ and 1.0 for 20Ni-5Co/Al_2O_3 were shown in Fig. S4. It should be pointed out that Eq. (4) was only used for quantitative comparison of the catalyst activity rather than providing reaction kinetics. Using a fixed reaction order of IPN for different catalysts, the catalyst activity can be solely described by the rate constant.

At the Ni-Co loading of $x = 2.5$, the rate constant k_r was 0.6×10^{-2} $mol^{0.2}$ $L^{-0.2}$ min^{-1}, which increased to 2.1×10^{-2} $mol^{0.2}$ $L^{-0.2}$ min^{-1} at Ni-Co loading of $x = 5$. When the Ni-Co loading further increased to $x = 10$, 20 and 20(SI), the Ni-Co/Al_2O_3 catalyst activity showed little change and the rate constant k_r was within the range of $2.2–2.8\times10^{-2}$ $mol^{0.2}$ $L^{-0.2}$ min^{-1}. The selectivity to *m*-XDA was enhanced with increasing Ni-Co loading. In particular, the selectivity to *m*-XDA over 20Ni-5Co/Al_2O_3 was 99.9%, which was 77.9% higher than that over 2.5Ni-0.625Co/Al_2O_3. The 20Ni-5Co/Al_2O_3(SI) catalyst was less selective than 20Ni-5Co/Al_2O_3, showing 90.3% selectivity to *m*-XDA. In this work, MS was used to identify the heavy species in the products. In our previous work [43], some typical MS spectra showed that the enhanced formation of higher amines was responsible for the low selectivity to *m*-XDA. Over 20Ni-5Co/Al_2O_3, the condensation reactions were effectively suppressed and very little higher amines were detected.

To further analyze the effect of Ni-Co loading, the catalyst acid amount, rate constant and selectivity to *m*-XDA based on the same metal amount were plotted as a function of Ni-Co loading in Fig. 5. The results showed that at the loading of $x \geq 5$, the increase of Ni-Co loading decreased

the acid amount, while the catalytic activity and selectivity to *m*-XDA were enhanced. For the *x*Ni-*y*Co/Al_2O_3 catalysts, there was a strong correlation between the acid amount and the catalytic performance. Verhaak et al. reported similar results that the acid sites on the supported Ni catalyst were responsible for the condensation reactions in acetonitrile hydrogenation [17]. In the present work, the enhanced activity and selectivity to *m*-XDA by increasing the Ni-Co loading was due to the weakened adsorption of imines on the catalytic sites caused by the suppressed acidity, which was resulted from the decreased exposure of Ni/Co aluminates. However, the catalytic performance of 2.5Ni-0.625Co/Al_2O_3 was an exception. Compared with 5Ni-1.25Co/Al_2O_3, 2.5Ni-0.625Co/Al_2O_3 had less acid amount, but had lower activity and selectivity to *m*-XDA. Since there was more exposure of the support surface at lower Ni-Co loading, the low activity and selectivity to *m*-XDA over 2.5Ni-0.625Co/Al_2O_3 should be attributed to the effect of other sites on the support surface, which will be discussed in detail below.

3.2.2. Effect of the nature of support

The SiO_2 supported catalysts were evaluated for IPN hydrogenation. The catalytic results are listed in Table 2. Different from the γ-Al_2O_3 supported catalysts, the rate constant k_r based on the same metal amount remained in the range of 1.9–2.6×10^{-2} $mol^{0.2}$ $L^{-0.2}$ min^{-1} for different Ni-Co loading and preparation method. With an increase in Ni-Co loading, the selectivity to *m*-XDA increased from 27.9% over 2.5Ni-0.625Co/SiO_2 to 99.9% over 20Ni-5Co/SiO_2. Similar to the γ-Al_2O_3 supported catalysts, 20Ni-5Co/SiO_2(SI) had a lower selectivity to *m*-XDA (88.7%) than 20Ni-5Co/SiO_2.

The catalyst acid amount, rate constant k_r and selectivity to *m*-XDA were plotted as a function of Ni-Co loading for the SiO_2 supported catalysts in Fig. 5. The Ni-Co/SiO_2 catalysts had

much lower acidity than the Ni-Co/Al_2O_3 catalysts, and had its highest acid amount at a lower loading of x = 2.5. The catalytic activity of Ni-Co/SiO_2 was little affected by the Ni-Co loading, while the selectivity to *m*-XDA increased with increasing Ni-Co loading. According to the XRD and H_2-TPR results, more NiO and Co_3O_4 and less $NiCo_2O_4$ and Ni/Co silicates were formed on SiO_2 than on γ-Al_2O_3, and the metal composition of the Ni-Co/SiO_2 catalysts was less dependent on the Ni-Co loading. As a result, xNi-yCo/SiO_2 at all Ni-Co loadings (x = 2.5–20) had low acidity and consequently similar catalytic activity. The differences in physicochemical properties of the xNi-yCo/SiO_2 and xNi-yCo/Al_2O_3 catalysts, which had important effects on the catalytic performance, could be attributed to the weaker metal-support interaction between Ni/Co and SiO_2.

Compared with the xNi-yCo/Al_2O_3 catalysts, the acid amount of xNi-yCo/SiO_2 based on the same metal amount was much lower. However, the correlation between the *m*-XDA selectivity and the Ni-Co loading was strong. To further investigate the effect of Ni-Co loading, MgO supported Ni-Co catalysts were also prepared and evaluated for IPN hydrogenation. The selectivity to *m*-XDA was 37.2% over 5Ni-1.25Co/MgO, which was lower than that over its counterparts on γ-Al_2O_3 and SiO_2, even though MgO is a typical basic support and 5Ni-1.25Co/MgO had no acidity (no significant NH_3 desorption peak was detected in the NH_3-TPD characterization). The above results, including the catalytic result of 2.5Ni-0.625Co/Al_2O_3, indicated that the catalyst acid amount was not the only factor that affected the *m*-XDA selectivity and some support sites other than acid sites could catalyze the side reactions. It was clear that the amount of exposed support sites decreased with the increase of Ni-Co loading, and for the results of xNi-yCo/SiO_2, the correlation between the amount of exposed support sites and *m*-XDA selectivity was more consistent and crucial than that between the acidity and *m*-XDA selectivity.

In conclusion, the selectivity to *m*-XDA was not only affected by the catalyst acid amount, but also affected by other sites on the support. The nature of support significantly affected the catalyst composition and physicochemical properties, and thus affected the catalytic performance. For *x*Ni-*y*Co/SiO_2, the catalyst acidity was in a very low range, and there was a more consistent correlation between the amount of exposed support sites and *m*-XDA selectivity. Compared with SiO_2, γ-Al_2O_3 has a stronger interaction with Ni/Co, leading to the formation of a larger amount of Ni/Co aluminates and higher catalyst acidity. In addition, the metal dispersion was higher and the synergy effects between Ni and Co by forming $NiCo_2O_4$ were stronger on γ-Al_2O_3, which increased the selectivity to *m*-XDA, especially at low Ni-Co loading.

3.2.3. Effect of the surface hydroxyl groups

It was reported in previous studies that the acid sites are the main catalytic sites for the condensation reactions in IPN hydrogenation. However, the results in this work showed that the catalyst acidity was not the only factor that affected *m*-XDA selectivity. As discussed in 3.2.1 and 3.2.2, low *m*-XDA selectivities were obtained over the supported catalysts with low metal loadings and high amounts of exposed support sites. In this work, the effects of these support sites were further studied by introducing bare supports, namely γ-Al_2O_3 and SiO_2, into the IPN hydrogenation system.

In the blank experiments of IPN hydrogenation using only the support, both γ-Al_2O_3 and SiO_2 had very low activity for the conversion of IPN. In additional experiments, a mixture of 1.25 g 20Ni-5Co/Al_2O_3(SI) and 8.75 g γ-Al_2O_3 was used. The results are shown in Fig. 6. The catalytic results of the mixture of 1.25 g 20Ni-5Co/SiO_2(SI) and 8.75 g SiO_2 were also included. Comparing the catalytic results, it was found that the rate constant k_r and *m*-XDA selectivity of the

mixture of 20Ni-5Co/Al_2O_3(SI) and γ-Al_2O_3 (1.1×10^{-2} $mol^{0.2}$ $L^{-0.2}$ min^{-1} and 38.1%, respectively) were lower than that of 20Ni-5Co/Al_2O_3(SI) (2.2×10^{-2} $mol^{0.2}$ $L^{-0.2}$ min^{-1} and 90.3%, respectively). Similar results were obtained with the mixture of 20Ni-5Co/SiO_2(SI) and SiO_2.

It has been well known that the surface hydroxyl groups, which widely existed on oxide supports, played an important role in adsorption and catalytic reaction [25-29]. To understand the possible effect of the surface hydroxyl groups, additional studies were carried out. According to the literature [44], the concentration of hydroxyl groups on the SiO_2 surface could be modified by treatment at different temperatures without significant change of other surface properties. In this study, the SiO_2 samples calcined at 400 ^oC and 600 ^oC for 4 h were each mixed with the reduced 20Ni-5Co/SiO_2(SI) and evaluated in the IPN hydrogenation reaction. The results were shown in Table 3. The BET surface area and the content of the surface hydroxyl groups were also tested and included in Table 3 and Fig. S5. The calcination treatment had important effect on the surface hydroxyl content and the catalytic performance, while the effect on the BET surface area was negligible and the acidity kept in a very low range. The untreated SiO_2 had a surface hydroxyl content of 0.59%, which decreased to 0.33% on the SiO_2 treated at 400 ^oC, and further decreased to 0.12% on the SiO_2 treated at 600 ^oC. With the decrease of the surface hydroxyl content, the *m*-XDA selectivity increased from 28.1% to 65.4%. This suggested that the surface hydroxyl groups were also the active sites for condensation side reactions.

To further study the roles of the surface sites, the spent catalyst and support were separated after the reaction and analyzed by TG-DTA. The results are shown in Fig. 7. The spent 20Ni-5Co/Al_2O_3(SI), 2.5Ni-0.625Co/Al_2O_3, 20Ni-5Co/SiO_2(SI) and 2.5Ni-0.625Co/SiO_2 catalysts were also analyzed for comparison (Fig. S6). As shown in the TG-DTA results, all the spent

catalysts and supports had weight loss peaks corresponding to the oxidation of heavy species deposited on the catalysts during the reaction. The weight loss peaks at the different temperatures were due to different heavy components formed on the catalyst. A smaller amount of heavy species was formed on the more selective catalyst and the weight loss peak appeared at lower temperature. For the spent mixture of 20Ni-5Co/Al_2O_3(SI) and γ-Al_2O_3, the catalyst and support were separately characterized by TG-DTA, showing that the weight loss peaks of 20Ni-5Co/Al_2O_3(SI) and γ-Al_2O_3 occurred at 365 ^oC and 485 ^oC, respectively. Similar results were obtained with the experiments using the spent mixture of 20Ni-5Co/SiO_2(SI) and SiO_2.

By combining the above results, the following reaction mechanism was proposed for the IPN hydrogenation reaction system: the hydrogenation reaction occurs on the metal sites of the catalyst, and the condensation reactions occur on the support sites, including the acid sites and the surface hydroxyl groups. Imines and amines are formed and desorbed from the metal sites, diffused in the liquid phase and re-adsorbed on these support sites, and finally produce heavy species by the condensation reaction on the acid sites and hydroxyl groups on the support surface.

4. Conclusions

The γ-Al_2O_3 and SiO_2 supported Ni-Co bimetallic catalysts with different metal loading were synthesized and evaluated for IPN hydrogenation. The repeated impregnation method (RI method) effectively facilitated metal dispersion as compared with the single step impregnation method (SI method). The physical morphology and crystal size of *x*Ni-*y*Co/Al_2O_3 prepared by the RI method were almost independent of the Ni-Co loading. The effect of catalyst acidity was confirmed by the study of the effect of the preparation method and Ni-Co loading of *x*Ni-*y*Co/Al_2O_3. However, besides the acid sites on the catalyst, the surface hydroxyl groups on the oxide supports also

catalyzed the condensation reactions. The enhanced selectivity to *m*-XDA by increasing the Ni-Co loading was attributed to the combined effect of the suppressed acidity and the decreased amount of exposed surface hydroxyl groups. The optimal 20Ni-5Co/Al_2O_3 and 20Ni-5Co/SiO_2 catalysts prepared by the RI method both have 99.9% selectivity to *m*-XDA in the presence of basic additives.

Acknowledgements

The authors gratefully acknowledge the financial supports by Program for New Century Excellent Talents in University of China (NCET-12-0297). They thank Prof. D. Z. Wang for helpful discussion and English revision.

References

1 S. W. Row, T. Y. Chae, K. S. Yoo, S. D. Lee, D. W. Lee, Y. Shul, *Can. J. Chem. Eng.*, 2007, **85**, 925-928.

2 T. Shi, H. Li, L.Yao, W. Ji, C. T. Au, *Appl. Catal., A.*, 2012, **425**, 68-73.

3 T. Y. Chae, S. W. Row, K. S. Yoo, S. D. Lee, D. W. Lee, *Bull. Korean Chem. Soc.*, 2006, **27**, 361-362.

4 B.W. Hoffer, J.A. Moulijn, *Appl. Catal., A.*, 2009, **352**, 193-201.

5 F. Hochard, H. Jobic, J.Massardier, A. J. Renouprez, *J. Mol. Catal. A-Chem.*, 1995, **95**,165-172.

6 P. Scharringer, T. Muller, J. Lercher, *J. Catal.*, 2008, **253**, 167-179.

7 *US Pat.*, 5 869 653, 1999.

8 B. W. Hoffer, *Tuning Raney-type and Supported Ni Catalysts for Commercial Hydrogenation Reactions*, 2003.

9 Y. Huang, W. M. H. Sachtler, *Appl. Catal., A.*, 1999, **182**, 365-378.

10 L. Hegedűs, T. Máthé, T. Kárpáti, *Appl. Catal., A.*, 2008, **349**, 40-45.

11 Y. Huang, *J. Catal.*, 2000, **190**, 69-74.

12 M.H.G. Prechtl, J.D. Scholten, J. Dupont, *J. Mol. Catal. A-Chem.*, 2009, **313**, 74-78.

13 P. Braos-Garcıa, P. Maireles-Torres, E.,Rodrıguez-Castellón, A.Jiménez-López, *J. Mol. Catal. A-Chem.*, 2003, **193**, 185-196.

14 G. D. Yadav, M.R. Kharkara, *Appl. Catal., A.*, 1995, **126**, 115-123.

15 D. J. Segobia, A. F. Trasarti, C.R. Apesteguía, *Appl. Catal., A.*, 2012, **445**, 69-75.

16 Y. Huang, M.M.H. Sachtler, *J. Catal.*, 1999, **188**, 215-225.

17 M. J. F. M. Verhaak, *Catal. Lett.*, 1994, **26**, 37-53.

18 C. V. Rode, M. Arai, M. Shirai, Y. Nishiyama, *Appl. Catal., A.*, 1997, **148**, 405-413.

19 A. Infantesmolina, *J. Catal.*, 2004, **225**, 479-488.

20 H. Chen, M. Xue, S. Hu, *J. Shen, Chem. Eng. J.*, 2012, **181**, 677-684.

21 R. K. Marella, K. S. Koppadi, Y.Jyothi, K. S. R. Rao, D. R. Burri, *New J. Chem.*, 2013, **37**, 3229.

22 C. De Bellefon, P. Fouilloux, *Catal. Rev.*, 1994, **36**, 459-506.

23 J. V. Braun, G. Blessing, F. Zobel, *Berichte der deutschen chemischen Gesellschaft (A and B Series)*, 1923, **56**, 1988-2001.

24 F. M. Cabello, D. Tichit, B. Coq, A. Vaccari, N. T. Dung, *J. Catal.*, 1997, **167**, 142-152.

25 A. Zecchina, C. Lamberti, S. Bordiga, *Catal. Today*, 1998, **41**, 169-177.

26 P. Ganesh, P.R.C. Kent, G.M. Veith, *J. Phys. Chem. Lett.*, 2011, **2**, 2918-2924.

27 R.G. Pavelko, H. Daly, M. Hübner, C. Hardacre, E. Llobet, *J. Phys. Chem. C.*, 2013, **117**, 4158-4167.

28 H. Liu, K.M. Liew, C. Pan, *Phys. Chem. Chem. Phys.*, 2013, **15**, 3866-80.

29 J. Zhu, J. Vanommen, L. Lefferts, *Catal. Today*, 2006, **117**, 163-167.

30 H. Valdés, R.F. Tardón, C.A. Zaror, *Chem. Eng. J.*, 2012, **211-212**, 388-395.

31 K. Tsutsumi, H. Emori, H. Takahashi, *B. Chem. Soc. Jpn.*, 1975, **48**, 2613-2617.

32 A. C. Gluhoi, P. Mărginean, U. Stănescu, *Appl. Catal., A.*, 2005, **294**, 208-214.

33 R. Mueller, H. K. Kammler, K. Wegner, S.E. Pratsinis, *Langmuir*, 2013, **19**, 160-165.

34 A. Gluhoi, N. Bogdanchikova, B. Nieuwenhuys, *J. Catal.*, 2005, **232**, 96-101.

35 A. A. Khassin, T. M. Yurieva, V. V. Kaichev, V. I. Bukhtiyarov, A. A. Budneva, E. A. Paukshtis, V. N. Parmon, *J. Mol. Catal. A-Chem.*, 2001, **175**, 189-204.

36 D. Xu, W. Li, H. Duan, Q. Ge, H. Xu, *Catal. Lett.*, 2005, **102**, 229-235.

37 P. De Bokx, W. Wassenberg, J. Geus, *J. Catal.*, 1987, **104**, 86-98.

38 H. Lu, H. Yin, Y. Liu, T. Jiang, L. Yu, *Catal. Commun.*, 2008, **10**, 313-316.

39 W. D. Mross, *Cat. Rev.*, 1983, **25**, 591-637.

40 S. Benbenek, E. Fedoryńska, P. Winiarek, *React. Kinet. Catal. Lett.*, 1993, **51**, 189-195.

41 W. Kania, K. Jurczyk, *Appl. Catal.*, 1987, **34**, 1-12.

42 V.L. Barrio, P.L. Arias, J.F. Cambra, M.B. Güemez, J.M. Campos-Martin, B. Pawelec, J.L.G. Fierro, *Appl. Catal., A.*, 2003, **248**, 211-225.

43 C. Liu, T.F. Wang, *RSC Adv.*, 2014, **109**, 63725-63733.

44 L.T. Zhuravlev, *Langmuir*, 1987, **3**, 316-318.

Table captions

Table 1. Physical properties of supported Ni-Co catalysts and supports

Table 2. Acidity and reaction results of *x*Ni-*y*Co/Al_2O_3 and *x*Ni-*y*Co/SiO_2

Table 3. Effect of calcination temperature on surface property, hydroxyl group content and catalytic performance of SiO_2

Table 1. Physical properties of supported Ni-Co catalysts and supports

Ni-Co loading *x* (wt%)	S ($m^2 g^{-1}$)	V_p ($cm^3 g^{-1}$)	D_p (nm)	Crystal size (nm)		
				NiO [a]	Co_3O_4 [b]	Co_2NiO_4 [c]
0[d]	221 (152)	0.63 (0.62)	7.92 (12.32)	/	/	/
2.5[d]	218 (144)	0.60 (0.59)	7.92 (12.36)	/ (19.6)	/ (19.9)	/ (20.9)
5[d]	209 (130)	0.57 (0.56)	7.88 (12.30)	/ (20.6)	/ (19.8)	/ (21.2)
10[d]	190 (123)	0.52 (0.49)	7.88 (12.28)	10.8 (22.4)	20.9 (20.3)	17.4 (22.4)
20[d]	153 (100)	0.41 (0.38)	7.90 (12.22)	11.4 (21.6)	21.0 (20.2)	16.9 (21.0)
20(SI)[d]	159 (96)	0.39 (0.37)	7.88 (12.28)	20.2 (34.9)	32.2 (24.8)	29.6 (27.2)

[a] Crystal size of NiO was calculated from the characteristic peak at 43 °.

[b] Crystal size of Co_3O_4 was calculated from the characteristic peak at 31 °.

[c] Crystal size of $NiCo_2O_4$ was calculated from the characteristic peak at 36 °.

[d] The numbers outside the brackets are the results of *x*Ni-*y*Co/Al_2O_3, and those in the brackets are the results of *x*Ni-*y*Co/SiO_2.

Table 2. Acidity and reaction results of *x*Ni-*y*Co/Al_2O_3 and *x*Ni-*y*Co/SiO_2[a]

Ni-Co loading, *x* (wt%)	Acidity (mmol NH_3 g^{-1})	k_r (10^{-2} $mol^{0.2}$ $L^{-0.2}$ min^{-1})	$S_{m\text{-XDA}}$ (%)
0	0.180 (0.014)	/	/
2.5[b]	0.224 (0.087)	0.6 (2.6)	22.0 (27.9)
5[b]	0.474 (0.061)	2.1 (2.0)	45.5 (45.8)
10[b]	0.346 (0.029)	2.4 (2.1)	96.5 (65.7)
20[b]	0.160 (0.023)	2.8 (2.2)	99.9 (99.9)
20(SI)[b]	0.264 (0.045)	2.2 (1.9)	90.3 (88.7)

[a] Reaction conditions: 80 °C, 6.0 MPa, catalyst in 200~400 μm containing 0.25 g Ni and 0.0625 g Co, 80 mL toluene and 20 mL methanol as solvent, 2.9 g IPN feed, 0.086 g NaOH, 180 mL min^{-1} hydrogen gas flow, 800 rpm stirring.

[b] The numbers outside the brackets are the results of *x*Ni-*y*Co/Al_2O_3, and those in the brackets are the results of *x*Ni-*y*Co/SiO_2.

Table 3. Effect of calcination temperature on surface property, hydroxyl group content and catalytic performance of SiO_2 [a]

Support	S (m^2 g^{-1})	Acidity (mmol NH_3 g^{-1})	Surface hydroxyl content (wt%)	$S_{m\text{-XDA}}$ (%)
SiO_2-untreated	152	0.014	0.59	28.1
SiO_2-400 [b]	149	0.005	0.33	42.3
SiO_2-600 [b]	150	0.004	0.12	65.4

[a] Reaction conditions: 80 °C, 6.0 MPa, 1.25 g 20Ni-5Co/SiO_2(SI) + 8.75 g SiO_2, both in 200~400 μm, 80 mL toluene and 20 mL methanol as solvent, 2.9 g IPN feed, 0.086 g NaOH, 180 mL min^{-1} hydrogen gas flow, 800 rpm stirring.

[b] SiO_2-400 and SiO_2-600 were the SiO_2 samples calcined at 400 °C and 600 °C for 4 h, respectively.

Scheme caption

Scheme 1. Reaction network of IPN hydrogenation reactions

Figure captions

Fig. 1. XRD results of: (a) *x*Ni-*y*Co/Al_2O_3 and γ-Al_2O_3; (b) *x*Ni-*y*Co/SiO_2 and SiO_2: (A) support, (B) *x*=2.5, (C) *x*=5, (D) *x*=10, (E) *x*=20, (F) *x*=20 (SI)

Fig. 2. SEM images of (a) γ-Al_2O_3, (b) 5Ni-1.25Co/Al_2O_3, (c) 20Ni-5Co/Al_2O_3, and (d) 20Ni-5Co/Al_2O_3(SI)

Fig. 3. H_2-TPR profiles of (a) *x*Ni-*y*Co/Al_2O_3, Ni/Al_2O_3 and Co/Al_2O_3; (b) *x*Ni-*y*Co/SiO_2: (1) *x*=2.5, (2) *x*=5, (3) *x*=10, (4) *x*=20, (5) *x*=20(SI)

Fig. 4. Catalytic performance of (a) (b) *x*Ni-*y*Co/Al_2O_3 and (c) (d) *x*Ni-*y*Co/SiO_2 catalysts

Fig. 5. Acidity, selectivity to *m*-XDA and rate constant of the supported Ni-Co catalyst: (a) acidty and selectivity to *m*-XDA, (b) acidity and rate constant k_r

Fig. 6. Comparison of catalytic performance of (a) 20Ni-5Co/Al_2O_3(SI) and (b) 20Ni-5Co/SiO_2(SI) catalysts with or without the introduction of bare support

Fig. 7. TG-DTA results of the separated catalysts and supports after reaction: (a) 20Ni-5Co/Al_2O_3(SI) separated from the mixture, (b) γ-Al_2O_3 separated from the mixture, (c) 20Ni-5Co/SiO_2(SI) separated from the mixture, (d) SiO_2 separated from the mixture

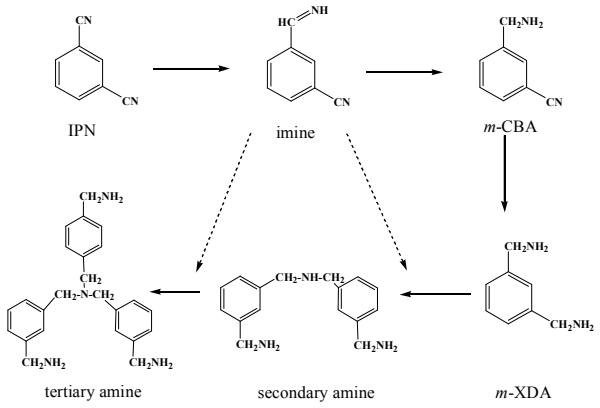

Scheme 1. Reaction network of IPN hydrogenation reactions

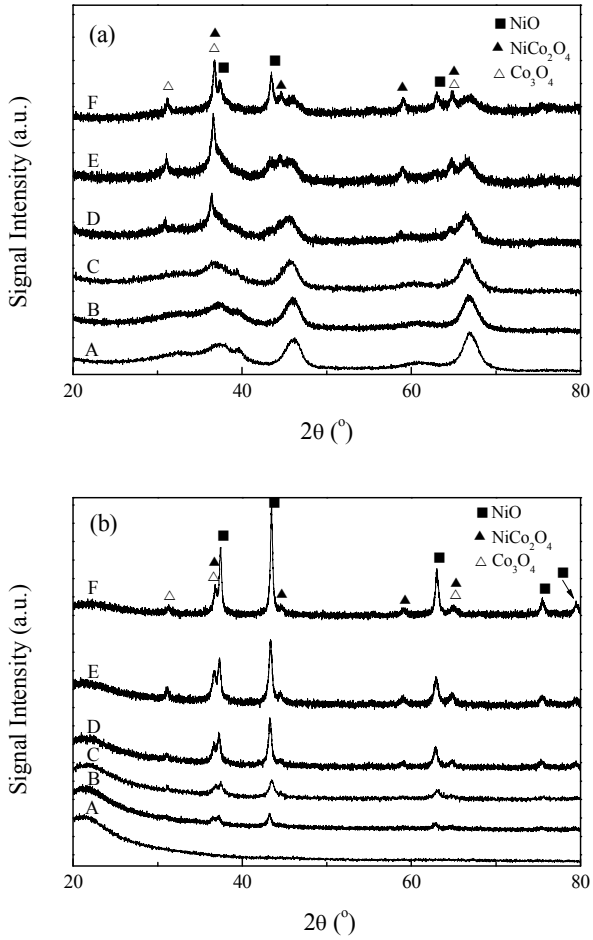

Fig. 1. XRD results of: (a) *x*Ni-*y*Co/Al_2O_3 and *γ*-Al_2O_3; (b) *x*Ni-*y*Co/SiO_2 and SiO_2: (A) support, (B) *x*=2.5, (C) *x*=5, (D) *x*=10, (E) *x*=20, (F) *x*=20 (SI)

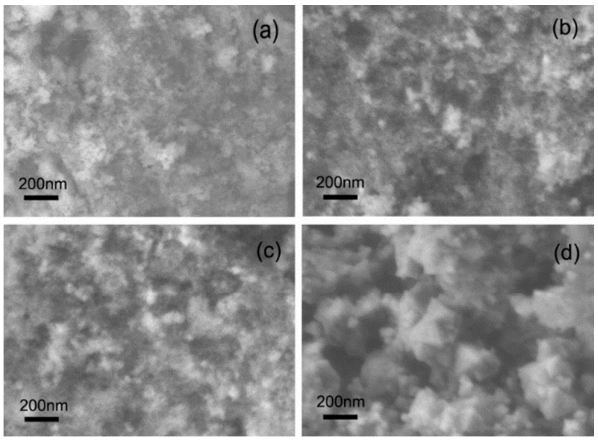

Fig. 2. SEM images of (a) γ-Al_2O_3, (b) 5Ni-1.25Co/Al_2O_3, (c) 20Ni-5Co/Al_2O_3, and (d) 20Ni-5Co/Al_2O_3(SI)

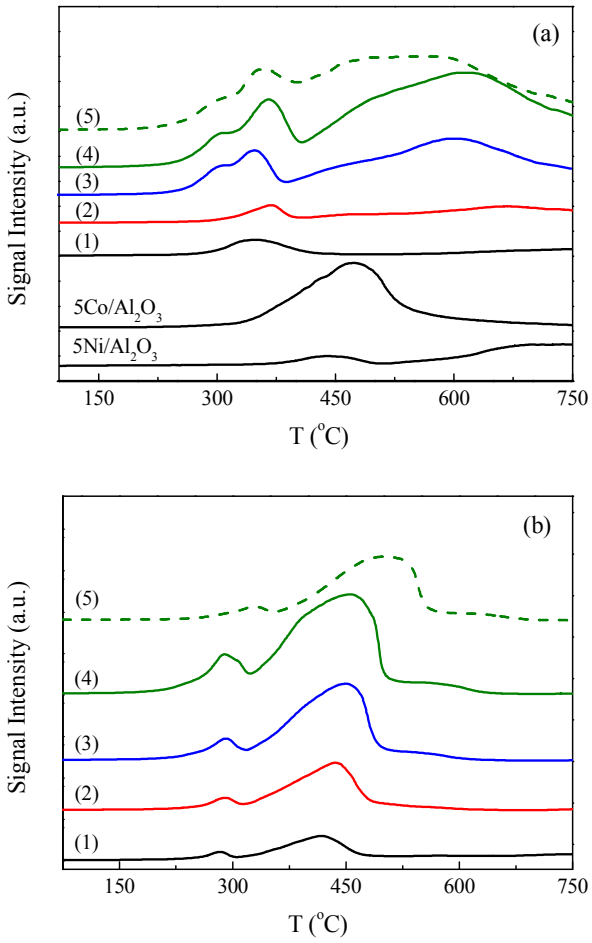

Fig. 3. H_2-TPR profiles of (a) *x*Ni-*y*Co/Al_2O_3, Ni/Al_2O_3 and Co/Al_2O_3; (b) *x*Ni-*y*Co/SiO_2: (1) *x*=2.5, (2) *x*=5, (3) *x*=10, (4) *x*=20, (5) *x*=20(SI)

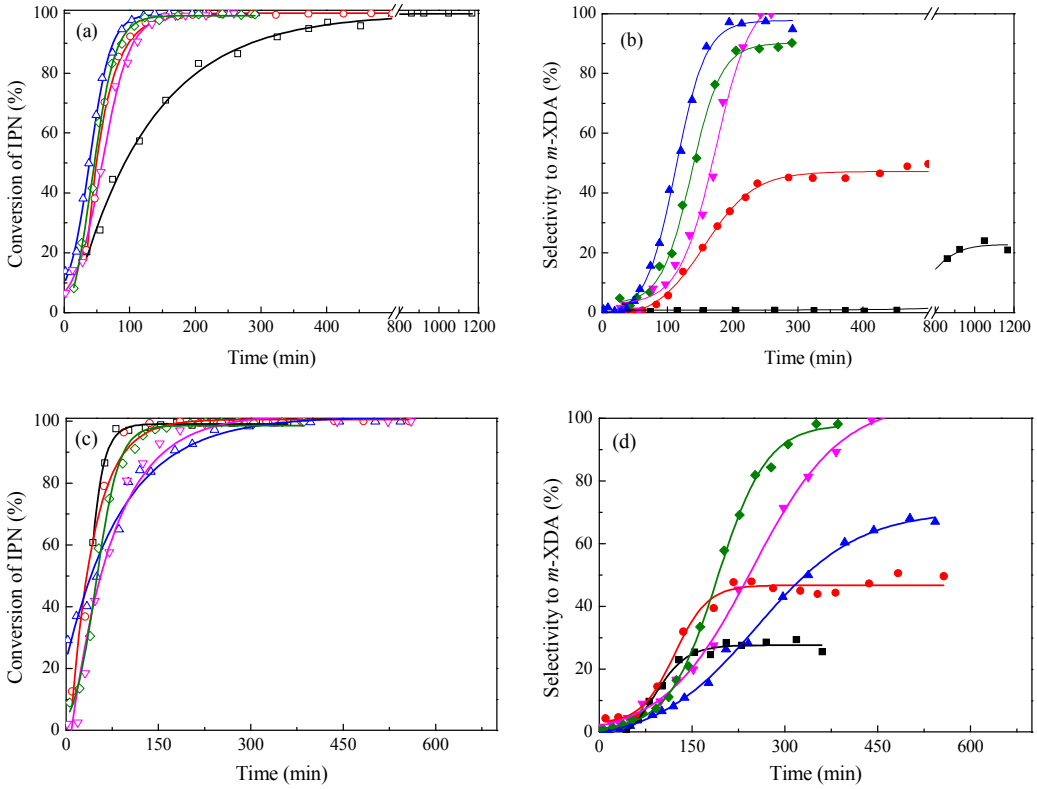

Fig. 4. Catalytic performance of (a) (b) *x*Ni-*y*Co/Al_2O_3 and (c) (d) *x*Ni-*y*Co/SiO_2 catalysts □■ *x*=2.5, ○● *x*=5, △▲ *x*=10, ▽▼ *x*=20, ◇◆ *x*=20(SI), open and solid symbols represent conversion and selectivity, respectively.

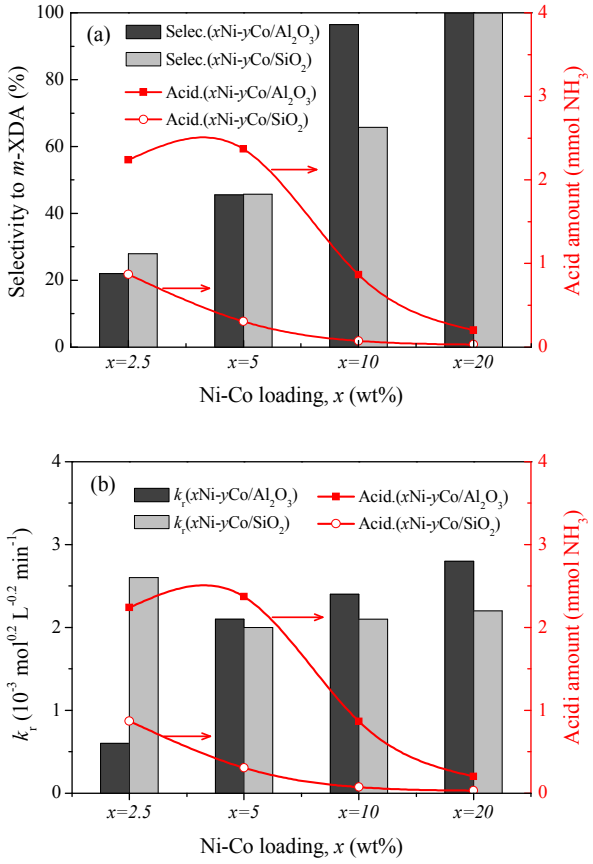

Fig. 5. Acidity, selectivity to *m*-XDA and rate constant of the supported Ni-Co catalyst: (a) acidty and selectivity to *m*-XDA, (b) acidity and rate constant k_r

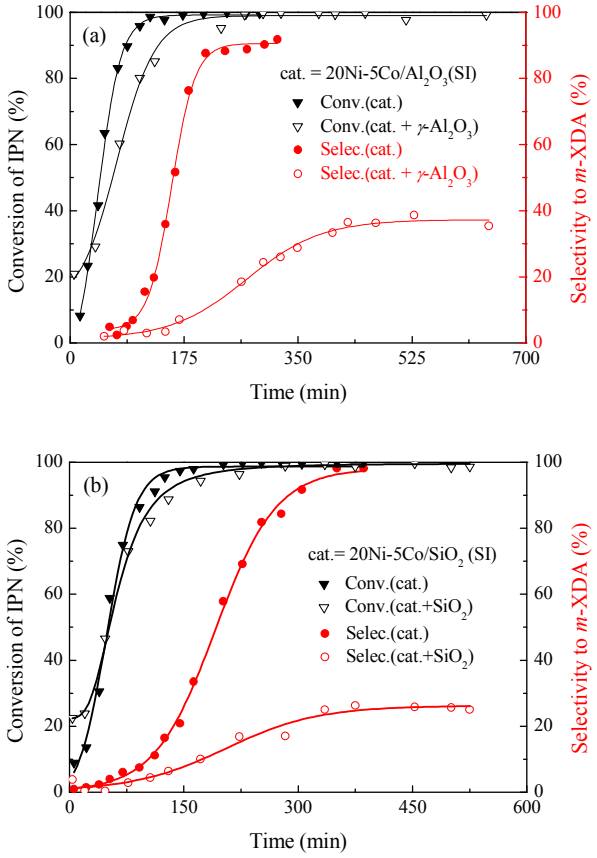

Fig. 6. Comparison of catalytic performance of (a) 20Ni-5Co/Al_2O_3(SI) and (b) 20Ni-5Co/SiO_2(SI) catalysts with or without the introduction of bare support

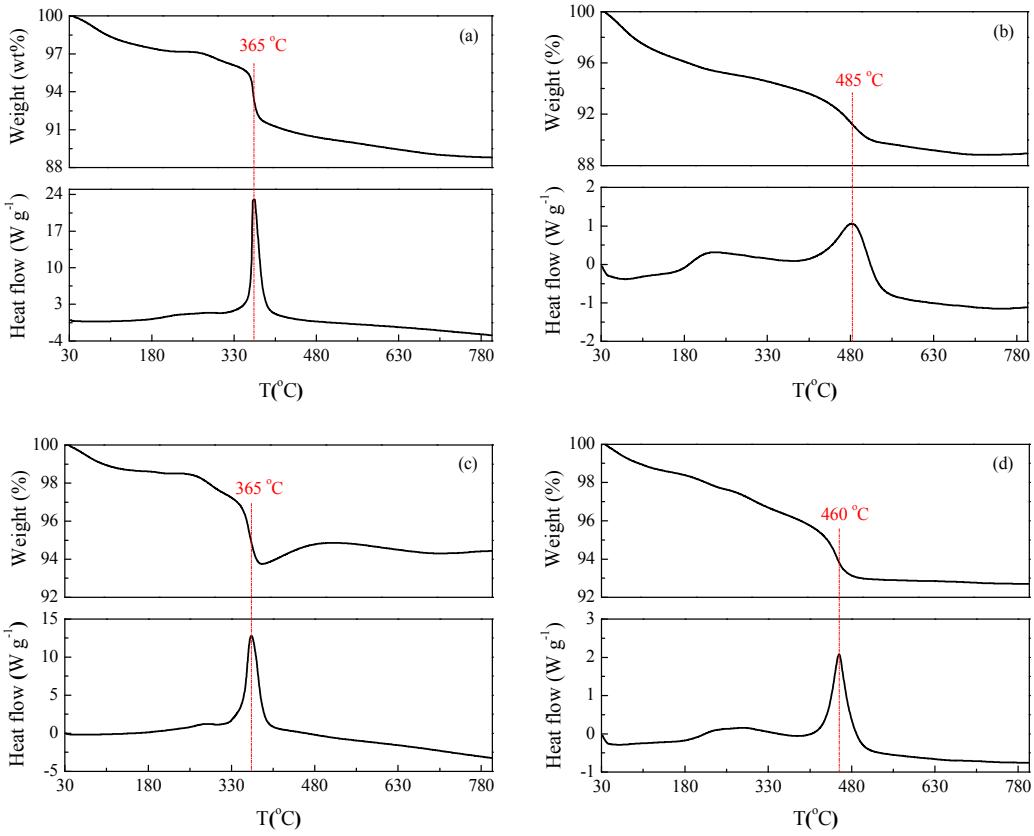

Fig. 7. TG-DTA results of the separated catalysts and supports after reaction

(a) 20Ni-5Co/Al_2O_3(SI) separated from the mixture, (b) γ-Al_2O_3 separated from the mixture,

(c) 20Ni-5Co/SiO_2(SI) separated from the mixture, (d) SiO_2 separated from the mixture